# Millisecond Pulsed Laser Micro-drilling of Stainless Steel – Optimizing Hole Quality Using Response Surface Methodology

Arvind Kumar Gupta, Ramesh Singh, and Deepak Marla*

Mechanical Engineering Department, Indian Institute of Technology Bombay, Mumbai-400076, India
*Corresponding author's e-mail: dmarla@iitb.ac.in

Quasi-continuous wave (QCW) fiber lasers have revolutionized micro-hole drilling in various industries by generating high-energy pulses lasting milliseconds. A single pulse of this laser can drill micro-holes with aspect ratios exceeding 10 on metal sheets ranging from 1-5 mm thick. However, challenges like hole taper and burr formation have limited their widespread adoption. Despite being introduced in 2011, there is limited research on drilling with QCW fiber lasers. To overcome the challenges, understanding hole quality and optimizing process parameters are required. Therefore, experiments have been conducted when pulse energy is greater than the threshold pulse energy of 3 mm thickness of the SS304 sample to identify an optimal range. A 2-factor, 3-level face-centered central composite design is employed to design experiments in the optimal power and pulse duration range. Optimal conditions were determined: a 308 μm minimum hole entry diameter at 3000 W power and 1 ms pulse width (yielding an aspect ratio of 10), a 0.38° minimum taper angle at 5902 W power and 8 ms pulse width, and a 39 μm minimum mean burr height at 4779 W power and 2 ms pulse width. These findings pave the path for enhanced methods to create superior quality micro-holes.

DOI: 10.2961/jlmn.2023.03.2012

**Keywords:** micro-drilling, QCW fiber laser, design of experiments, taper, burr, optimization

## 1. Introduction

Improving the manufacturing processes is essential for enhancing the complexities of everyday objects. In various industries such as aerospace, μ-electronics, bio-medical, and automobile, there is a growing need for advancements in micro-drilling. This entails achieving diameters ranging from a few microns to several hundred microns, along with a high aspect ratio. The demand for such capabilities has been stimulated by the market's increasing appetite for smaller and more efficient devices, thus driving interest in the field of micromachining [1,2]. The evolution of laser drilling is leading to advancements in both productivity and accuracy. Specifically, millisecond pulsed laser drilling is widely employed in the manufacturing industry to create holes in metals and alloys ranging in size from 0.25 to 1 mm. This well-established technology is particularly valuable in the production of various components in aero-engines. One of its notable advantages is the ability to effectively drill hard-to-machine materials at challenging angles [3]. A notable trend in turbine design involves incorporating a higher number of cooling mechanisms, resulting in decreased fuel efficiency. As an example, a gas turbine afterburner typically features approximately 40,000 holes, each with a diameter of 0.5 mm [4]. It is envisioned that future aero engines will surpass 150,000 cooling holes, further emphasizing the importance of cooling systems in optimizing performance and efficiency [5]. Hence, it becomes essential to minimize hole defects in laser drilling techniques. These techniques enable the production of high aspect ratio micro-holes at high speeds, emphasizing the need for improved precision and quality control in the manufacturing process. A QCW laser can drill in a thick plate using a single pulse. It can have pulse energy up to 1000 J, pulse width up to 50 ms, and frequency up to 50 kHz. It can be provided in both pulsed and CW mode and has higher wall-plug efficiency. Despite being introduced in 2011, there are little research has been done.

However, there are extensive research has been undertaken to investigate hole taper and burr formation at the hole's exit, using other lasers like CW laser, $CO_2$ laser, Nd:YAG laser, and ultrashort lasers. The paragraph highlights several noteworthy studies conducted on the topic. In a study by K. P. Singh et al. [6], the focus was on examining the hole taper of a 1.2 mm thick Kelver-19 composite through drilling using Nd:YAG laser. Through the utilization of Taguchi's methodology, the researchers optimized process parameters such as lamp current and air pressure. The study concluded that air pressure had the most significant influence on hole taper. M. Ghoreishi et al. [7] conducted a study to investigate the influence of controllable process parameters on hole taper and circularity in Nd:YAG laser multiple-pulse drilling. Their research examined the effects of lamp current, pulse frequency, air pressure, and specimen thickness. Additionally, R. Biswas et al. [8] examined the impacts of lamp current, pulse frequency, air pressure, and specimen thickness on hole circularity and taper in drilling using Nd:YAG laser. In the $CO_2$ laser drilling of titanium alloy, S. Chatterjee et al. [9] conducted an experimental study to examine the effects of machining process parameters, including laser power, frequency, and flushing pressure. Their research focused on analyzing the impact of these parameters on hole taper, heat-affected zone (HAZ), and spatter area. The study also involved optimization techniques to enhance the drilling process. The exploration of production rate, energy consumption per unit of material removal rate (MRR),

and hole quality performance in different drilling techniques (single-shot, multi-shot, and trepanning) utilizing quasi-continuous wave (QCW) fiber laser on Inconel 718 specimens was conducted by S. Sarfraz et al. [10]. The study focused on investigating the influence of process parameters on taper. The impact of the bowl-bottom effect on hole taper in deep hole drilling of CFRP (Carbon Fiber Reinforced Polymer) composites using an ultra-fast laser was investigated by N. Tao et al. [11]. The study concluded that the emergence of the bowl-bottom effect is attributed to the divergence of the irradiated beam and secondary processing. W. Ouyang et al. [12] explored the double rotation cutting technique in a picosecond laser drilling process on CFRP composite. It is found that there is an absence of burr and fracture at the hole with minimal hole taper 0.64°. In their study, Cao et al. [13] examined the occurrence of burr formation during drilling operations using Nd:YAG laser and explored methods to reduce it. Their approach involved utilizing laser ablation guided by a water jet. The researchers hypothesized that the material could be ablated effectively through plasma detonation and supported this hypothesis through experimental investigations. Wang et al. [14] focused on studying the reduction of taper in plasma micro drilling induced by picosecond laser on CFRP (carbon fiber reinforced polymer) plates. Their findings indicated that this particular process led to a reduction in hole taper of approximately 32% when compared to the conventional laser drilling process conducted in ambient air. Shin et al. [15] explored the concept of taper control through the utilization of multilevel femtosecond laser processing. Zhang et al. [16] conducted research on minimizing hole taper in the femtosecond laser drilling method by employing a two-step approach. The results indicated that the taper angle could be reduced by up to 4° using this method. Liu et al. [17] focused on optimizing taper in fiber laser trepanning drilling by employing various techniques such as Taguchi's orthogonal array, analysis of variance, regression modeling, and multi-objective genetic algorithm. Their study aimed to achieve an optimal taper through the integration of these methodologies. Their findings revealed that defocusing had a greater impact on taper compared to the heat-affected zone (HAZ). N. K. Sreejith et al. [18] conducted research to optimize the hole taper by utilizing an integrated grey Taguchi-based response surface methodology using Nd:YAG laser. Through their investigations, they observed that the crucial process parameters for achieving the desired hole taper were the lamp current and air pressure. D. Pramanik et al. [19] focused on analyzing and optimizing the hole taper under low-power laser conditions using fiber laser. Similarly, S. Pattanayak et al. [20] conducted an investigation into hole taper in laser microdrilling using Nd:YAG laser, specifically employing argon as an assist gas. They successfully identified the critical process parameters and utilized grey relational analysis for optimization purposes. Additionally, H. Wang et al. [21] explored the drilling quality by employing water-to-air as a medium and Nd:YAG laser as source. Their findings indicated a noticeable improvement in hole taper as a result of their experimental approach.

Although there is enough work on optimization of laser drilling process, research on QCW fiber laser drilling is very limited because it is developed recently. Specifically, this research aims to optimize taper angle, burr, and diameter utilizing a single millisecond pulse drilling technique.

The study presented in the paper initially focused on conducting a series of experiments to establish the correlation between pulse energy and both hole depth and threshold pulse energy for a specific specimen thickness. Subsequently, another set of experiments was carried out to examine hole taper and burr within the range surpassing the threshold values for various sample thicknesses. Based on the findings from these investigations, an optimal range was determined. Building upon this, a designed set of experiments utilizing CCD-RSM (Central Composite Design-Response Surface Methodology) was conducted to optimize the diameter, taper, and burr height parameters.

## 2. Experimental setup

The experiments were conducted using a long pulse ytterbium laser system (YLS)-600/6000-quasi-continuous wave (QCW)-air-cooled (AC) fiber laser from IPG Photonics. This laser system emits radiation at a wavelength of 1070nm, which is invisible to the naked eye. The laser beam profile is top-hat in shape. In continuous-wave mode, it can deliver a maximum power output of 600 W, while in pulsed mode, the power output can reach up to 6090 W. The pulse duration of the laser can be adjusted from 0.1 ms to 10 ms, and the pulse repetition rate can range from 1 Hz to 500 Hz. The laser beam spot diameter is 125 μm.

**Table 1** Specifications of laser setup.

| Parameters | Typical value |
|---|---|
| Laser beam profile | Top-hat |
| Laser wavelength | 1070 nm |
| Laser spot diameter | 125 μm |
| Focal length | 125 mm |
| Beam parameter product (BPP) | 4.0 mm·mrad |
| Beam quality ($M^2$) | 11.74 |
| Pulse peak power | 6000 W |
| Maximal pulse energy | 60 J |
| Pulse duration | 0.1-10 ms |
| Frequency | 1-500 Hz |
| Maximal average power | 600 W |
| Gas type | Compressed air |

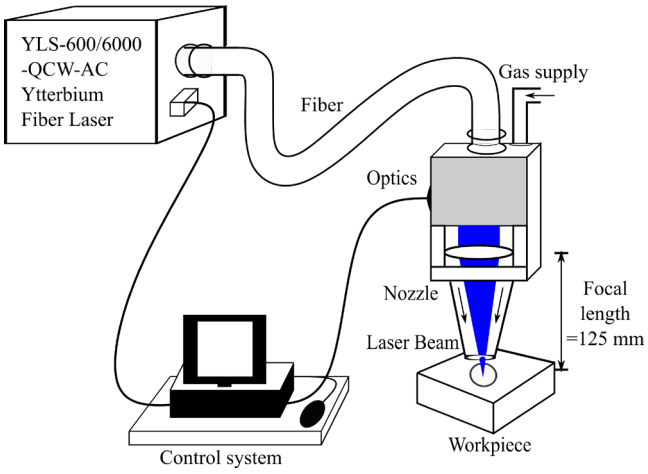


**Fig.1** Experimental setup.

In addition to the primary laser, a red guide laser operates at a wavelength of 635 nm with a power output of less than 1 mW. This guide laser assists in alignment and positioning. The setup has a depth of focus of 399 μm, allowing for a specific range of distances within which the laser remains focused. The laser beam quality factor ($M^2$) is measured to be 11.74, considering an output fiber core diameter of 100 μm. The assist gas employed is compressed air, with a flow rate of $4.86 \times 10^{-3}$ m$^3$ / s at a flow pressure of 5 bar. For detailed specifications of the setup, refer to Table 1. Furthermore, a schematic diagram illustrating the setup can be found in Figure 1. In the experiments, Stainless Steel 304 was selected as the material for the sample. The samples used were 20 mm squares obtained by cutting from plates of thickness 3.0 mm. These samples were prepared using a wire-cut EDM and cleaned with Acetone. To assess the flatness error of the samples, a random selection was made from the batch of samples, and these were measured using a coordinate measuring machine (CMM). The average flatness error was determined to be 4.7 μm, which was smaller than the experimental setup's depth of focus (399 μm). As a result, this level of flatness error, caused by the sample's warpage, bend, or tilt, does not impact hole quality when the laser source nozzle moves from one point to another within the sample for processing. To evaluate the quality of the drilled holes, an Alicona Infinity Focus Profilometer and SEM (Scanning Electron Microscopy) were used. The experiments employed the single-pulse drilling technique, where the critical laser process parameters were peak power, pulse width, and pulse energy. The performance parameters analyzed for the main hole quality included depth, diameter, taper, and burr. The experiments covered a range of laser pulse peak powers, ranging from 1000 W to 6090 W. The pulse duration varied from 1 ms to 10 ms, and the laser pulse energy ranged from 1 J to 60 J. Six holes were drilled for each operating parameter to assess repeatability and minimize random errors.

## 3. Optimization methodology

The experiments were designed using the central composite design (CCD), which is a response surface methodology (RSM) approach [22]. Design of experiments (DOEs) was conducted in Minitab software by utilizing an unblocked and full CCD to determine the optimal laser process parameters: pulse peak power (P), pulse duration ($\boldsymbol{t_{on}}$), and pulse energy ($\boldsymbol{E_p}$). To optimize the hole depth, diameter, taper angle, and burr height, the pulse power ranged from a minimum of 3000 W to a maximum of 6090 W. Similarly, the pulse duration varied from 1 ms to 9.9 ms. The DOEs were executed using the face-CCD method, resulting in 13 experimental runs. These runs consisted of four cube points, five center points within the cube, and four axial center points. During the DOEs, the runs were randomized, and each experiment was performed once without replicates. The designed experiments are given in Table 2. The data obtained from the conducted experiments were analyzed using Minitab 17 software. A confidence level of 95% was set for all intervals in the analysis. Hence, the negligible p-value is 0.05. Three types of confidence intervals were utilized: two-sided, lower bound, and upper bound. No Box-Cox transformations were deemed necessary for the analysis. None of the options of stepwise, forward selection, and backward elimination were selected. The term "full quadratic" was chosen from the available options, which included linear, linear plus squares, linear plus interactions, and full quadratic. Various graphs were employed in the analysis, such as residuals plots versus fits and order. The analysis results encompassed simple and expanded tables of the method, analysis of variance (ANOVA), model summary, coefficients, regression equation, fits, and diagnostics.

**Table 2** Design of experiments.

| Factor | Symbol | Level | | |
|---|---|---|---|---|
| | | -1 | 0 | +1 |
| Power (W) | P | 3000 | 4545 | 6090 |
| Pulse width (ms) | $t_{on}$ | 1 | 4.45 | 9.9 |

The flowchart presented in Figure 2 calculates the objective function and desirability for the optimization process. In this flowchart, Z represents the set of process parameters, and F is the primary objective function that relates to the process parameters through function f. Additionally, there are single objective functions, $f_1$, $f_2$, $f_3$, and $f_4$, which are used to minimize the hole diameter, burr height, and taper angle, respectively. The desirability function is employed to determine the desirability of a particular value, with DR representing its value ranging from 0 to 1. Values closer to 1 indicate a higher level of desirability. It is important to note that the desirability function assists in finding the optimal value within the set of 13 experimental runs. However, one drawback is that it does not provide the globally optimum value.

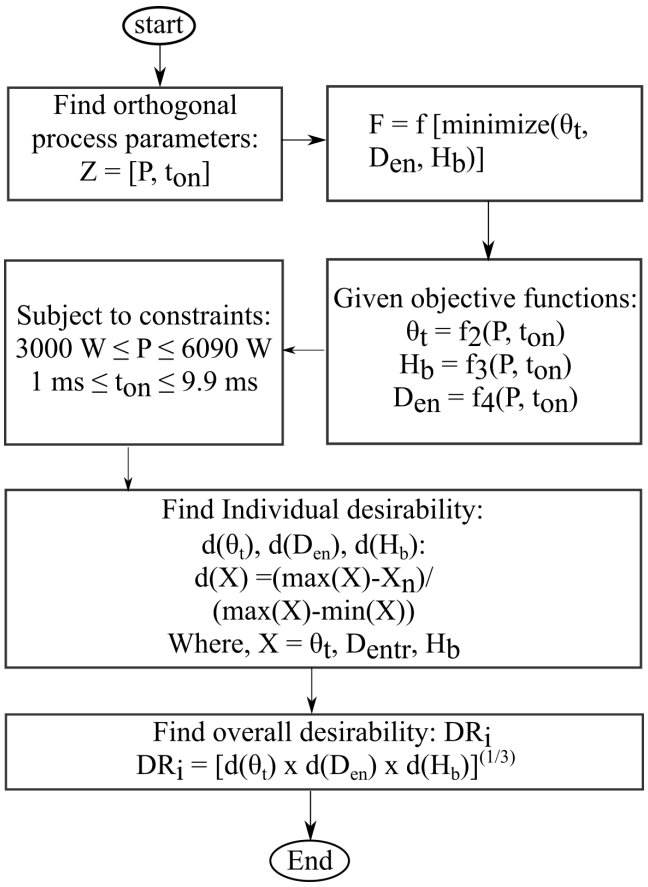


**Fig. 2** Flowchart for desirability evaluation.

To overcome this drawback, a response surface methodology (RSM) modelling is conducted once again, considering the overall desirability as a function of pulse power (P) and pulse duration ($t_{on}$). By incorporating these factors, the new objective function is formulated as follows:

$$D = f_5(P, t_{on}) \quad (1)$$

The optimal values of the process parameters were successfully obtained by converting the multi-objective optimization problem into a single-objective optimization problem.

## 4. Results and discussion

The experiments were conducted on stainless steel 304 specimens using the YLS-600/6000-QCW-AC series CW ytterbium fiber laser. A single-pulse laser drilling technique was employed, where the laser beam was focused on the specimen's top surface. The results of hole characteristics include hole diameter at the entrance and the exit, taper angle, and burr height at the entrance (hump) and the exit. Furthermore, the results of optimization are presented.

### 4.1 Hole characteristics

The main focus of the investigation revolved around analyzing the characteristics of the holes. These characteristics encompassed the diameter of the hole at both the entrance ($D_{en}$) and the exit ($D_{ex}$) points, the taper angle ($\theta_t$), hump height ($H_h$) at the hole entrance, and the burr height ($H_b$) observed explicitly at the hole exit as shown in figure 3. Since, similar results have been obtained for diameter at the entry and the exit, and burr at the entry (hump) and the exit. Therefore, results of the entrance diameter ($D_{en}$) and burr height at the exit ($H_b$) have been given in following paragraphs.

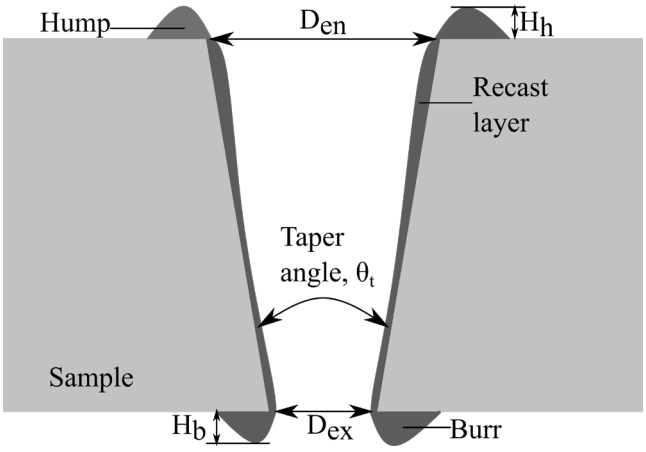


**Fig. 3** Laser drilling process.

#### 4.1.1 Entry and exit diameters

In Figure 4, an SEM image of the hole at the entrance is presented. The image clearly reveals the presence of a hump formation and spatter around the edges of the hole. These structures are attributed to the removal of material in a molten form, resulting from the generation of high temperatures exceeding the critical temperature of the specimen material due to the intense laser beam. Furthermore, it is observed that the circularity of the hole at the entrance is notably good. This is likely due to the consistent and uniform transportation of molten material during the drilling process. It is observed the entry diameter (402 µm) is greater than the beam diameter because of laser high energy diffusion and melt-expulsion along with vaporization material removal mechanism due to metal vapor pressure and Marangoni convection [21]. It is also concluded that melt-expulsion plays a significant role in the process as hump formation took place at the top surface of the hole.

Figure 5 showcases key characteristics of the hole exit through a scanning electron microscopy (SEM) image. The circularity of the hole at the exit appears to be of moderate quality in the image. This observed variation is primarily attributed to the uneven distribution of burrs encircling the hole exit. The irregular distribution of burrs is a consequence of varying recoil pressure from metal vapor along both the radial and azimuthal directions of the hole. Consequently, this uneven distribution leads to a non-uniform dispersion of melt-ejected materials encircling the hole's periphery when the final layer of molten material remains within the hole cavity and an opening is present at the hole exit [23].

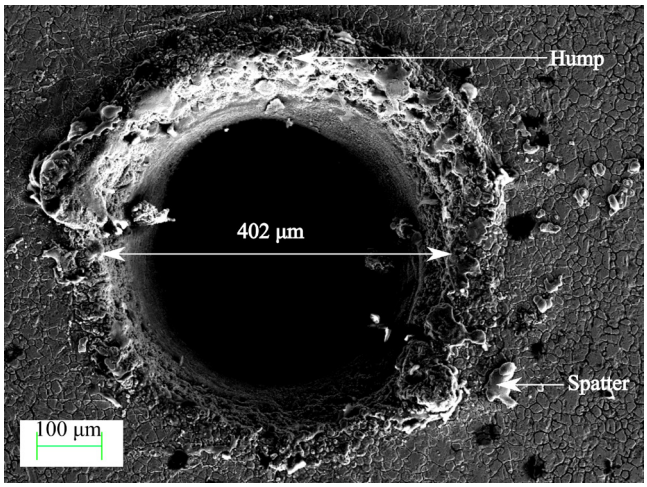


**Fig. 4** SEM image of the entrance of the hole.

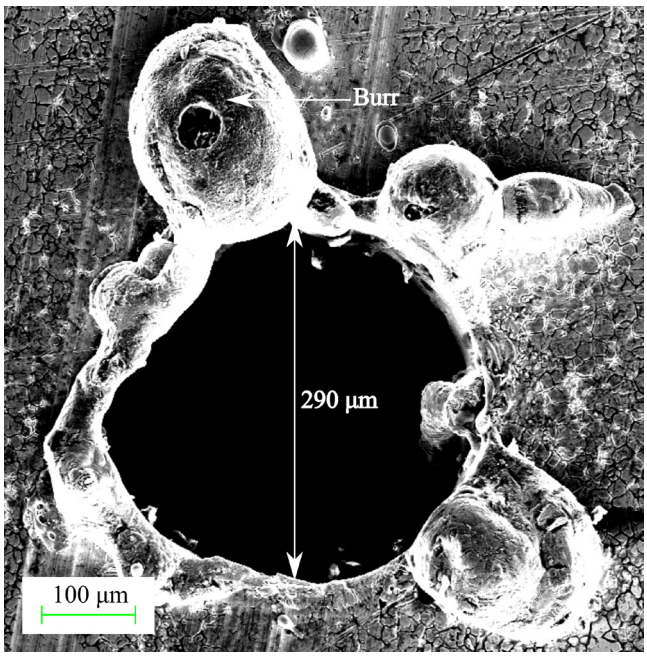


**Fig. 5** SEM image of the exit of the hole.

In Figure 6, the hole diameters at both the entrance and the exit are presented alongside the corresponding laser pulse energy. The pulse energy varies in the range of 15 J to 60 J, and it is worth noting that the entire range surpasses the threshold pulse energy required for drilling through the hole in a 3 mm thick SS304 sample. The threshold pulse energy denotes the minimum energy necessary to create a hole that penetrates a specific thickness of the sample. During the analysis, it was noted that the hole diameter at both the entrance and the exit demonstrated comparable increasing trends in relation to the pulse energy. However, beyond a certain threshold value of pulse energy, the diameter at the exit exceeded that at the entrance.

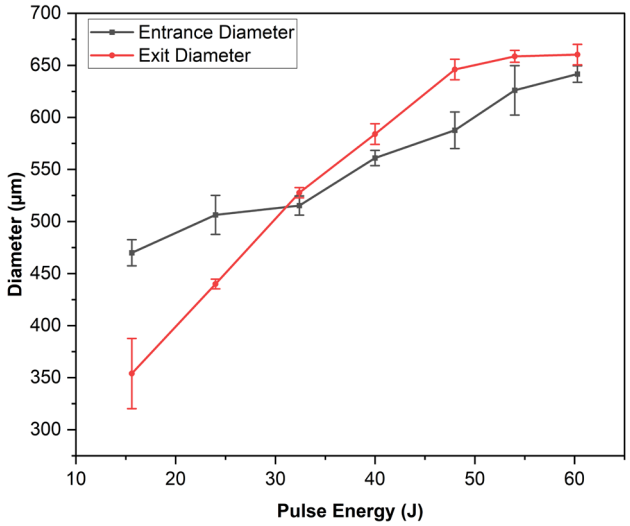


**Fig. 6** Diameter with pulse energy at pulse width of 1 ms.

This phenomenon can be attributed to the increased availability of heat energy at the exit as the pulse energy rises. Furthermore, it was observed consistently that the hole diameter remained higher than the spot diameter of the laser beam, indicating that the drilling process resulted in an enlargement of the hole beyond the initial beam size.

### 4.1.2 Hole taper

In the single-pulse laser drilling process, hole taper is an inherent machining challenge caused by the natural divergence of the laser beam. Consequently, minimizing the magnitude of the hole taper is desirable to enhance the functionality of the drilled hole. Therefore, investigations have been carried out beyond the threshold pulse energy to examine the variation in taper within these areas. This series of experiments encompassed the range from the threshold laser energy up to 10 times the threshold laser energy, focusing on specimens with a specific thickness. The Taper angle ($\theta_t$) is calculated in degrees by using equation 2;

$$\theta_t = \tan^{-1}\left[\frac{(D_1 - D_2)}{2t}\right] \times \frac{180}{\pi} \quad (2)$$

Where $D_1$ and $D_2$ are the average diameter of the hole at the entrance and the exit, respectively, and $t$ is the thickness of the specimen.

Figure 7 shows an SEM image of the sectional view of the hole. It clearly shows a tapered profile along the hole depth. Figure 8 depicts the variation of the hole taper in relation to pulse energy. A positive taper angle indicates convergence, while a negative taper angle signifies divergence of the hole. The experimental findings demonstrate that the taper angle decreases, transitioning from convergent to divergent hole internal taper profile. Then, the taper increases in divergent

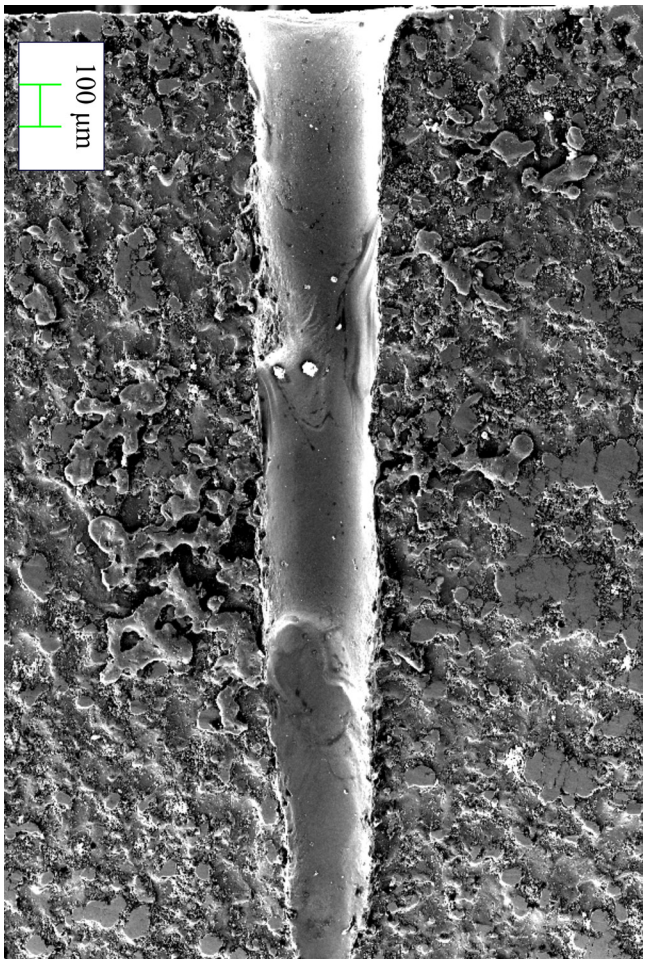


**Fig. 7** SEM image of the sectional view of the hole.

profile after a certain value of pulse energy. A similar observation has been drawn from Figure 6. From Figure 9, the schematic diagram shows how the taper hole was created systematically. The reason behind this variation can be attributed to the distribution of pulse energy. At lower pulse energies, the majority of the energy is consumed at the entrance of the hole, resulting in a higher increase in the entrance diameter compared to the exit diameter, as shown in the schematic figure. The figure clearly shows that after absorption of the laser beam, it is transferred from there to the vicinity area by the heat conduction method. A melt pool is formed when the temperature exceeds the melting point temperature. An upper layer of the melt pool gets vaporized when it gets further energy. Hence, metal vapor forms. This metal vapor exerted pressure on the melt pool along with Marangoni convection which was exerted due to temperature gradient along the depth of the melt pool. This leads to melt-expulsion at the periphery of the hole. That appears in the form of a hump. As depth increases, the melt expulsion mechanism becomes less efficient. When pulse energy increases above a certain value, plasma and assist gas pressure remove some amount of molten metal from the exit of the hole if a small opening exit there. This molten metal appeared in the form of a burr around a hole as shown in figure 5. Therefore, the exit diameter starts increasing at a higher

rate, and the taper angle decreases. This causes the rate of increase in the exit diameter to surpass that of the entrance diameter.

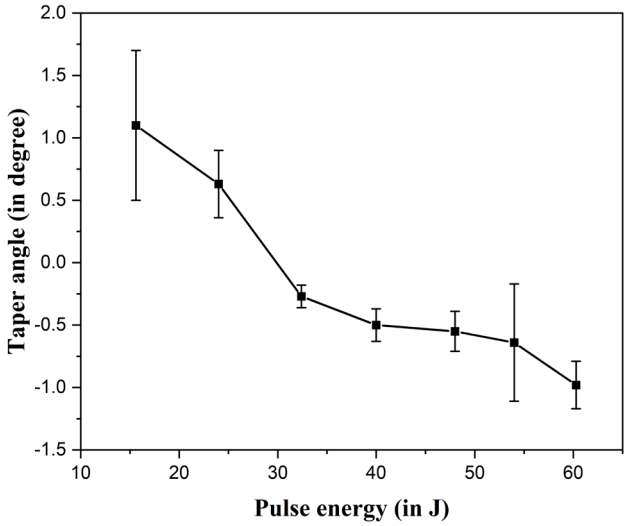


**Fig. 8** Hole taper with pulse energy at pulse width of 1 ms.

Hence, the taper profile changes from convergent to divergent. Interestingly, the results also demonstrated the possibility of obtaining a zero-taper angle under specific conditions. Furthermore, experiments involving variations in the focus position showed that the threshold pulse energy for a 3 mm thickness sample increases when the focus position is adjusted from the top to the bottom surface. Variations in defocus also play a role in altering the shape of the taper.

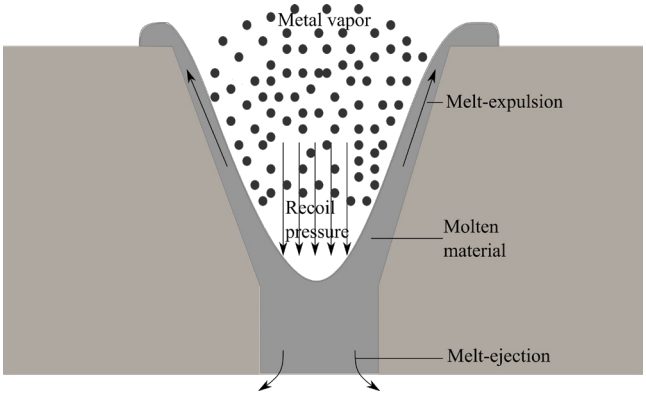


**Fig. 9** Schematic diagram for material removal mechanism.

**4.1.3 Burr of hole**

Burr is also an inherent manufacturing challenge associated with deep through-hole drilling, particularly when the laser beam exceeds a specific threshold fluence. Consequently, an experimental study was conducted to identify the influential process parameters and their distribution at the hole exit. The mean burr height ($H_b$) is determined by measuring the approximate area of the distributed burr and the average diameter at the hole exit. This information is then utilized in equation 3 to calculate the mean burr height;

$$H_b = \frac{A}{\pi D_2} \quad (3)$$

Here, $A$ represents the approximated burr distributed area, and $D_2$ is the exit diameter.

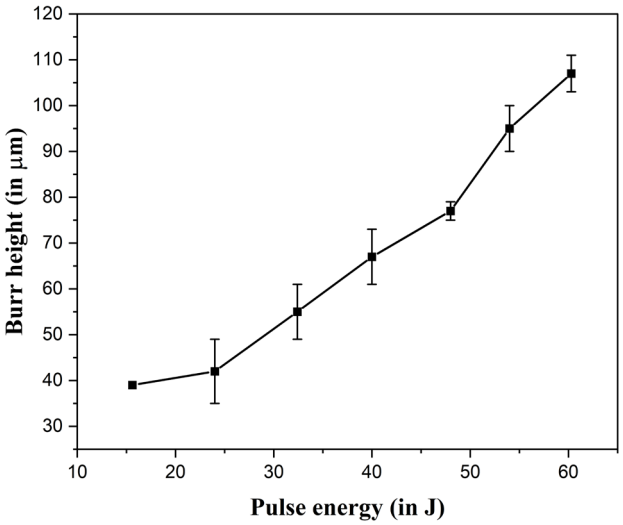


**Fig. 10** Burr with pulse energy at pulse width of 1 ms.

Figure 5 shows an SEM image of the exit of the hole. It shows the distribution of burr at the exit of the hole. Figure 10 illustrates the variation of burr at the hole exit in relation to pulse energy. The mean burr height demonstrates an increasing trend with pulse energy. However, there is a change in the increment rate for the mean burr height plots after a specific pulse energy value of the laser beam. This change in the increment rate is attributed to the dominant influence of the melt-ejection mechanism due to recoil pressure enhancement beyond the specific pulse energy threshold as shown in Figure 9.

**Table 3** Individual and composite desirability of hole quality.

| P (W) | $t_{on}(ms)$ | $E_p(J)$ | $D_{en}(\mu m)$ | $\theta_t(deg.)$ | $H_b\ (\mu m)$ | d($D_{en}$) | d($\theta_t$) | d($H_b$) | DR |
|---|---|---|---|---|---|---|---|---|---|
| 4545 | 5.45 | 24.77 | 506 | 0.63 | 26 | 0.338 | 0.656 | 0.87 | 0.577 |
| 4545 | 9.9 | 44.99 | 568 | -0.55 | 38 | 0.119 | 0.909 | 0.741 | 0.431 |
| 3000 | 1 | 3 | 318 | 3.69 | 14 | 1 | 0 | 1 | 0 |
| 3000 | 9.9 | 29.7 | 514 | 2.33 | 28 | 0.309 | 0.291 | 0.849 | 0.424 |
| 4545 | 1 | 4.54 | 340 | 0.43 | 18 | 0.922 | 0.699 | 0.956 | 0.85 |
| 6090 | 1 | 6.09 | 360 | 1.29 | 21 | 0.852 | 0.515 | 0.924 | 0.74 |
| 6090 | 9.9 | 60.29 | 602 | 0.1 | 107 | 0 | 0.77 | 0 | 0 |
| 4545 | 5.45 | 24.77 | 506 | 0.63 | 26 | 0.338 | 0.656 | 0.87 | 0.577 |
| 4545 | 5.45 | 24.77 | 506 | 0.63 | 26 | 0.338 | 0.656 | 0.87 | 0.577 |
| 6090 | 5.45 | 33.19 | 516 | -0.97 | 32 | 0.302 | 1 | 0.806 | 0.624 |
| 3000 | 5.45 | 16.35 | 470 | 1.1 | 24 | 0.464 | 0.555 | 0.892 | 0.612 |
| 4545 | 5.45 | 24.77 | 506 | 0.63 | 26 | 0.338 | 0.656 | 0.87 | 0.577 |
| 4545 | 5.45 | 24.77 | 506 | 0.63 | 26 | 0.338 | 0.656 | 0.87 | 0.577 |

### 4.2 Optimization of hole quality

Table 3 describes the individual desirability corresponding response variables like diameter ($D_{en}$), taper angle ($\theta_t$), and burr height ($H_b$) and overall desirability (DR) at the designed experiment conditions. It is shown that single-objective optimization can be converted into multi-objective optimization using the value of DR. This study tells the hole characteristics minimizing without any constraints, emphasizing process capability. However, it is possible to extend this to an additional study pertaining to minimizing taper, keeping other hole characteristic constraints. Such a study is not performed in this work. Depending on the functionality requirements, an optimization can be framed to minimize or maximize particular characteristics by imposing other constraints.

**Table 4** Revised ANOVA of diameter at the entrance of the hole.

| Source | Degree of freedom | Adj Sum of squares | Adj Mean squares | F-Value | P-Value |
|---|---|---|---|---|---|
| Model | 4 | 87161.1 | 21790 | 184.65 | 0.000 |
| Linear | 2 | 78518.7 | 39259 | 332.67 | 0.000 |
| P | 1 | 4592.7 | 4592.7 | 38.92 | 0.000 |
| $t_{on}$ | 1 | 73926 | 73926 | 626.43 | 0.000 |
| Square | 2 | 8642.5 | 4321.2 | 36.62 | 0.000 |
| P·P | 1 | 395.4 | 395.4 | 3.35 | 0.105 |
| $t_{on} \cdot t_{on}$ | 1 | 5835.4 | 5835.4 | 49.45 | 0.000 |
| Error | 8 | 944.1 | 118 | | |
| Lack-of-fit | 4 | 944.1 | 236 | | |
| Pure error | 4 | 0 | 0 | | |
| Total | 12 | 88105.2 | | | |
| R-sq = | 98.9% | R-sq(ad) | =98% | R-sq(pr) | =95% |

Table 4 presents the findings of the analysis of variance conducted on the hole entrance diameter. It can be inferred from the results that the pulse power has the highest p-value of 0.105. Consequently, the laser pulse peak power plays a significant role in altering the diameter. As the peak power increases, the amount of laser energy absorbed for heating also rises. This increased heat is then more efficiently conducted towards the entrance of the generating hole and its immediate surroundings. As a result, a majority of the material is primarily removed from the entrance of the hole due to the shorter heating duration, typically in milliseconds. Thus, it can be concluded that peak power has the most significant impact on the diameter of the hole's entrance. Equation 4 provides a comprehensive quadratic fitting relationship, which can be utilized to estimate the hole diameter value during the intermediate combination process parameters. Mathematically, it can be given by following the regression equation of diameter (in µm), $D_{en}$;

$$D_{en} = 114.5 + 0.0635P + 50.24t_{on} - 0.000005P^2 - 2.321t_{0n}^2 \quad (4)$$

The analysis of variance (ANOVA) results for the hole taper angle are presented in Table 5. Upon examination of the table, it becomes apparent that the highest p-value, 0.284, corresponds to the pulse width. This result indicates that the duration of the laser pulses is a significant factor influencing the taper angle. An increase in pulse duration leads to an increase in both pulse energy and heating time. This consequence enables more efficiently conducted absorbed heat to penetrate deeper along the hole's depth and reach the hole's exit. Subsequently, a deeper molten pool is created and gets molten material more time to flow out of the generating hole, accentuating the dominance of the melt ejection mechanism in removing material from the hole's exit. Consequently, the exit diameter expands, and the disparity between the entrance and exit diameters of the hole decreases, reducing the hole's taper angle. Thus, pulse duration has the greatest effect on the taper angle. Equation 5 represents a complete quadratic fitting relationship that captures the interplay between peak power, pulse duration, and diameter, thus providing insights into the alteration of the taper angle. It is mathematically given by following the regression equation of the taper angle (in degree), $\theta_t$;

$$\theta_t = 10.51 - 0.00313P - 0.411t_{on} + 0.0000001P^2 + 0.0256t_{on}^2 \quad (5)$$

**Table 5** Revised ANOVA of average hole taper angle.

| Source | Degree of freedom | Adj Sum of squares | Adj Mean squares | F-Value | P-Value |
|---|---|---|---|---|---|
| Model | 4 | 12.4583 | 3.11458 | 5.81 | 0.017 |
| Linear | 2 | 9.5585 | 4.77924 | 8.91 | 0.009 |
| P | 1 | 7.4817 | 7.48167 | 13.95 | 0.006 |
| $t_{on}$ | 1 | 2.0768 | 2.07682 | 3.87 | 0.085 |
| Square | 2 | 2.8998 | 1.44992 | 2.70 | 0.127 |
| P·P | 1 | 1.0998 | 1.09980 | 2.05 | 0.190 |
| $t_{on} \cdot t_{on}$ | 1 | 0.7072 | 0.70724 | 1.32 | 0.284 |
| Error | 8 | 4.2893 | 0.53617 | | |
| Lack-of-fit | 4 | 4.2893 | 0.53617 | | |
| Pure error | 4 | 0 | 0 | | |
| Total | 12 | 16.7477 | | | |
| R-sq = | 74.39% | R-sq(ad) | =61.58% | | |

A revised analysis of variance for the mean burr height is presented in Table 6. Upon examination of the table, it is evident that the highest p-value of 0.256 is associated with the square of pulse power and pulse duration, representing the laser pulse energy.

**Table 6** Revised ANOVA of mean burr height at the exit of the hole.

| Source | Degree of freedom | Adj Sum of squares | Adj Mean squares | F-Value | P-Value |
|---|---|---|---|---|---|
| Model | 5 | 5744.68 | 1148.94 | 9.85 | 0.005 |
| Linear | 2 | 3872.67 | 1936.33 | 16.61 | 0.002 |
| P | 1 | 1472.67 | 1472.67 | 12.63 | 0.009 |
| $t_{on}$ | 1 | 2400 | 2400 | 20.59 | 0.003 |
| Square | 2 | 576.01 | 288.01 | 2.47 | 0.154 |
| P·P | 1 | 178.29 | 178.29 | 1.53 | 0.256 |
| $t_{on} \cdot t_{on}$ | 1 | 178.29 | 178.29 | 1.53 | 0.256 |
| 2-way interaction | 1 | 1296 | 1296 | 11.12 | 0.013 |
| P· $t_{on}$ | 1 | 1296 | 1296 | 11.12 | 0.013 |
| Error | 7 | 816.09 | 116.58 | | |
| Lack-of-fit | 3 | 816.09 | 272.03 | | |
| Pure error | 4 | 0 | 0 | | |
| Total | 12 | 6560.77 | | | |
| R-sq = | 87.56% | R-sq(ad) | =78.68% | | |

This finding concludes that the laser pulse energy is the most influential process parameter in determining the burr height. As pulse energy increases, a larger quantity of heat is conducted deeper into the material, causing a deeper melt pool to form and intensifying the plasma generation. This heightened plasma generation leads to an increased generation of

recoil pressure from the metal vapor. This enhanced recoil pressure aids in expelling molten material from the exit point, resulting in a higher height for the resulting burr. Therefore, it can be concluded that pulse energy has the greatest effect on burr height. Equation 6 provides a quadratic fitting relationship between the process parameters pulse power and pulse duration and the evaluation parameter of hole quality, which is the burr height. The fitting relationship can be mathematically expressed by the following regression equation for burr height (in µm), $H_b$;

$$H_b = 100.1 - 0.0347P - 11.83t_{on} + 0.000003P^2 + 0.406t_{on}^2 + 0.002618P \cdot t_{on} \quad (6)$$

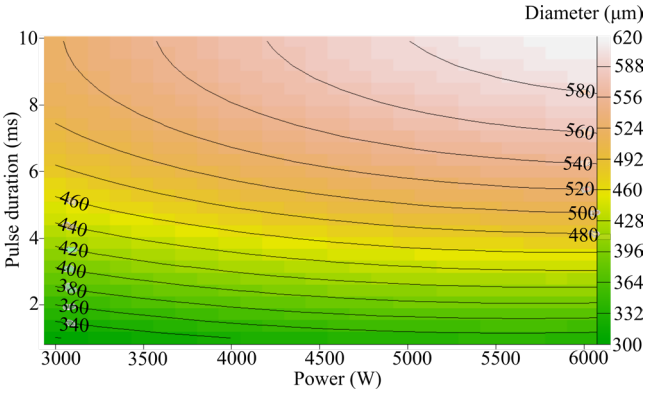


**Fig. 11** Contours of hole diameter at the entrance.

In Figure 11, the contours display various entrance hole diameter values in relation to pulse peak power and duration. The figure highlights a green region representing the desired area for achieving a minimum diameter. Within this desirable region, the peak power ranges from 3000 W to 6090 W, the pulse duration ranges from 1 ms to 4 ms, and the diameter ranges from 300 µm to 396 µm. It presents the optimization analysis of hole diameter, revealing that the minimum diameter achieved is 308 µm. This optimal diameter is obtained at a pulse power of 3000 W and a pulse width of 1 ms, resulting in a pulse energy of 3 J. The composite desirability for this particular outcome is 1.0.

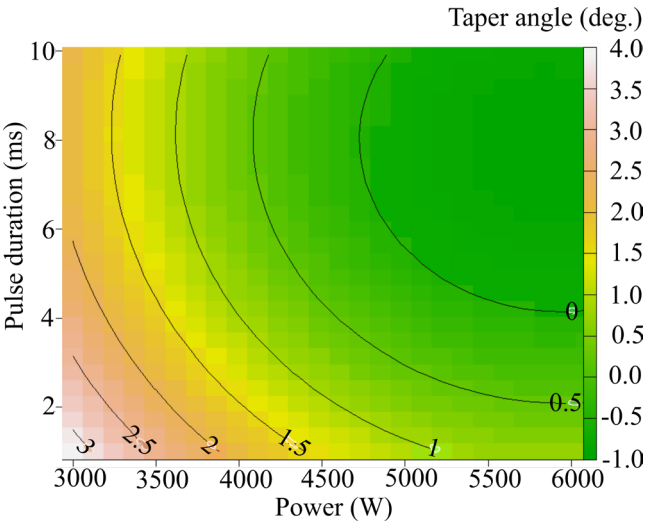


**Fig. 12** Contours of hole taper angle.

Figure 12 displays the contours of the taper angle against peak power and pulse duration. Within the figure, the green region represents the desired area for achieving a lower hole taper angle. The desirable region is defined by pulse peak power ranging from 3500 W to 6090 W, pulse duration ranging from 2 ms to 10 ms, and hole taper angle ranging from 1° to 0°. It is illustrated that from optimization analysis of the taper angle of the hole. It can be observed from the figure that the minimum taper angle achieved is -0.38°. This optimal taper angle is attained at a peak power of 5902 W and a pulse duration of 8 ms. The composite desirability at this optimal point is calculated to be 0.873. It is worth noting that a taper angle of zero is not considered an optimal value due to the sign conventions assigned to distinguish between convergent and divergent shapes of the hole taper.

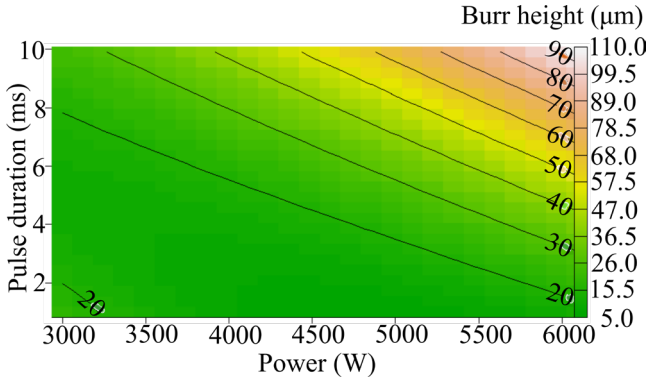


**Fig. 13** Contours of burr height.

Figure 13 presents the contours of the mean burr height against peak power and pulse duration. The green region indicates the desirable area for achieving the minimum average burr height in the figure. This desirable region is bounded by pulse peak power ranging from 3000 W to 6000 W, pulse duration ranging from 1 ms to 4 ms, and mean burr height ranging from 5 µm to 37 µm. It is depicted from optimization results for the mean burr height at the exit of the hole, that the minimum average burr height achieved is 39 µm, which occurs at a laser pulse peak power of 4779 W and a pulse duration of 2 ms. The composite desirability at this optimal point is calculated to be 1.0.

## 5. Conclusions

This research establishes the optimal operational parameters for a 3 mm SS304 specimen based on experimentation. The experiments were conducted by exceeding the specimen's threshold pulse energy and identifying the optimal range of laser parameters. The determined optimal range for peak power falls within 3000 W to 6000 W, while the pulse duration should vary from 1 ms to 10 ms in order to minimize diameter, taper, and burr height. The experiments were thoughtfully designed within this optimal range using the Central Composite Design (CCD) as a Response Surface Methodology (RSM) technique. Based on the investigation conducted, it can be concluded that it is possible to drill micro-holes with an aspect ratio of 10 in a 3 mm thick plate of SS. This can be achieved by utilizing a single pulse from a millisecond pulsed QCW fiber laser. The range of taper angles observed for these holes falls between 0° and 4°. To achieve these desirable results, specific parameters were found to be effective. The laser's power determines the hole's diameter, while the pulse width influences the taper angle. The power and pulse duration play an important role in

determining the burr height. The following optimal values for the parameters related to hole quality were determined through an optimization process: the minimum taper angle required is 0.38°, the minimum entrance diameter should be 308 μm, and the minimum burr height should be 39 μm.

**Acknowledgments**

We gratefully acknowledge the support provided by SERB-DST (Department of Science and Technology, Government of India) through RD/0119-DST0000-006, which has greatly aided in the execution of this study.

**References**

[1] M. Hasan, J. Zhao, and Z. Jiang: J. Manufactur. Process., 29, (2017) 343.
[2] P. Rana, A. Singh, A. Kottantharayil, and D. Marla: Manufactur. Lett., 35, (2023) 58.
[3] S. Marimuthu, M. Antar, J. Dunleavey, D. Chantzis, W. Darlington, and P. Hayward: Opt. Laser Tech., 94, (2017) 119.
[4] M.H.H. Van Dijk, D. de Vilrger, and J.E. Brouwer: Proc. 6th Conf. lasers Manufactur., (1989) 237.
[5] M. Antar, D. Chantzis, S. Marimuthu, and P. Hayward: Proc. Cirp, 42, (2016) 526.
[6] K.P. Singh, A. Bahl, G. Norkey, and G.D. Gautam: Mat. Today: Proc., 56, (2022) 3325.
[7] M. Ghoreishi, D.K.Y. Low, and L. Li: Int. J. Machine Tools Manufactur., 42, (2002) 985.
[8] R. Biswas, A.S. Kuar, S. Sarkar, and S. Mitra: Opt. Laser Tech., 42, (2010) 23.
[9] S. Chatterjee, S.S. Mahapatra, A. Mondal, and K. Abhishek: Sādhanā, 43, (2018) 1.
[10] S. Sarfraz, E. Shehab, K. Salonitis, and W. Suder: Energies, 12, (2019) 4610.
[11] N. Tao, G. Chen, W. Fang, and M. Li: Comp. Struct., 305, (2023) 116498.
[12] W. Ouyang, J. Jiao, Z. Xu, H. Xia, Y. Ye, Q. Zou, R. Tian, and L. Sheng: Opt. Laser Tech., 142, (2021) 107238.
[13] Z. Cao, H. Qiao, Y. Zhang, Y. Chen, and J. Zhao: J. Manufactur. Process., 77, (2022) 809.
[14] P. Wang, Z. Zhang, D. Liu, W. Qiu, Y. Zhang, and G. Zhang: Opt. Laser Tech., 151, (2022) 108022.
[15] S. Shin, W. Lee, J.K. Park, and D.H. Kim: Opt. Laser Tech., 159, (2023) 108956.
[16] F. Zhang, J. Wang, X. Wang, J. Zhang, Y. Hayasaki, D. Kim, and S. Sun: Opt. Laser Tech., 143, (2021) 107335.
[17] C. Liu, X. Zhang, L. Gao, X. Jiang, C. Li, and T. Yang: Optik, 242, (2021) 167186.
[18] N.K. Sreejith and R.D. Kumar: Mat. Today: Proc., 47, (2021) 5410.
[19] D. Pramanik, A.S. Kuar, S. Sarkar, and S. Mitra: Mat. Today: Proc., 26, (2020) 689.
[20] S. Pattanayak, S. Panda, and D. Dhupal: J. Manufactur. Process., 52, (2020) 220.
[21] H. Wang, G. Xu, S. Zhu, W. Zhou, N. Ren, and K. Xia: J. Manufactur. Process., 36, (2018) 175.
[22] D. Bhartiya, P. Rana, M.A. Singh, and D. Marla: J. Micro-and Nano-Manufactur., 8, (2020) 041006.
[23] D. Marla: "Laser Machining of Metals In: Adv. Machining Sci. (1st ed.), Ch. 7" ed. by V.K. Jain, (CRC Press, United States, 2022) 159.

(Received: July 10, 2023, Accepted: November 19, 2023)